

Interface modulation and quantum well to quantum wire crossover in semiconductor heterostructures

T. G. Dargam

Instituto de Física, Universidade Federal Fluminense, 24210-340, Niterói-RJ, Brazil

R. B. Capaz and Belita Koiller

Instituto de Física, Universidade Federal do Rio de Janeiro Cx. Postal 68.528, Rio de Janeiro, 21945-970, Brazil

(Received 5 February 2001; revised manuscript received 16 August 2001; published 7 December 2001)

We consider AlAs/GaAs/AlAs (001) quantum wells in which one of the interfaces is planar and the other is modulated by periodic steps. The systems are described theoretically within a real-space tight-binding approach, and the optical nature of the heterostructures is investigated through the calculated oscillator strength of the fundamental transition in the well. The interface profile amplitude and wavelength combined effects lead to distinct optical regimes, which are qualitatively summarized in a simple phase diagram. At short wavelengths, increasing the modulation amplitude causes a decrease in the oscillator strength and eventually a sharp direct-to-indirect gap transition takes place at a critical amplitude. For long enough wavelengths, the gap remains direct at all amplitudes: The oscillator strength decreases until it attains a minimum, and then it increases again as the interface modulation amplitude increases. The oscillator strength minimum in the second regime is a signature of a quantum well to quantum wire crossover in the optical behavior of the system.

DOI: 10.1103/PhysRevB.64.245327

PACS number(s): 78.67.-n, 73.22.-f, 78.66.Fd, 73.61.Ey

I. INTRODUCTION

The advances in crystal fabrication techniques allow the growth of heterostructures combining a wide variety of semiconductor materials of different atomic compositions. Semiconductor heterostructures, such as quantum wells (QW's), quantum wires, and quantum dots, remain continually in focus over recent decades. In particular, the study of interfaces between different materials have received considerable attention. Several experimental studies show that some degree of interface disorder is intrinsic to all epitaxial growth processes.^{1,2} Transport phenomena in heterostructures, such as the electron scattering rate, are sensitive to any degree of interface roughness.^{3,4} Moreover, two-dimensional quantum well width fluctuations lead to naturally formed lower-dimensional wells at interfaces. Optical measurements on QW's reveal interesting properties associated to these formations.⁵⁻⁸ Since optical phenomena in heterostructures are now widely implemented in technology,⁹ a better understanding of interface roughness effects in the optical properties of these systems is useful for further development of the field.

From the theoretical point of view, the envelope function approximation¹⁰ (EFA) provides a simple scheme for the treatment of optical and electronic properties of heterostructures. Nevertheless, a detailed description of the disorder region at heterointerfaces is known to be outside the range of applicability of this formalism. This type of study requires an atomistic description of the materials, and it was shown that the tight-binding (TB) model is well suited for modeling quantum heterostructures in situations where the EFA breaks down.¹¹ In this way, a simple empirical method based on the TB model and large supercells has been used to study different manifestations of interface imperfections, such as surface segregation,¹² diffusion,¹³ and the natural occurrence of roughness at interfaces.¹⁵ An interesting result that emerges

from all these studies is that small interface imperfections are usually negligible in affecting optical properties.¹⁴

Previous TB studies of interface roughness effects¹⁵ considered AlAs/GaAs/AlAs (001) QW's of average width W in which one of the interfaces is flat and the other has a shape given by an arbitrary oscillating function Z . At each interface, the material changes abruptly from GaAs to AlAs, or vice versa. Calculations were limited to periodically oscillating shape functions Z of comparable wavelengths. It was shown that the optical properties do not depend on the geometric details of Z , but only on the interface roughness,

$$\rho = \sqrt{\langle (Z - \langle Z \rangle)^2 \rangle}, \quad (1)$$

where $\langle \dots \rangle$ denotes averaging over the x - y plane, perpendicular to $z = [001]$, thus $\langle Z \rangle$ is the average interface height and ρ quantifies the *rms* deviation of the interface with respect to $\langle Z \rangle$.

In the present work we further explore this problem including the effects of the Z -function periodicity, i.e., oscillation wavelength. Given our previous results, a single functional dependence is considered, which we choose to be a periodic step function. Experimental studies¹ of AlAs/GaAs heterostructures grown along z indicate steps and terraces formation at interfaces preferentially along the $\eta = [\bar{1}10]$ direction. Motivated by these results, most results presented below refer to interface shape function with steps along η .

The optical nature of the heterostructures is described by the calculated oscillator strength f of the fundamental transition in the systems. We start with an optically active QW ($f \neq 0$) with flat interfaces and width W . When steps are present in one of the interfaces, increasing their amplitude up to $A = W$ leads to a quantum wire geometry (see Fig. 1). We show that, according to the steps periodicity λ , certain configurations become inactive ($f = 0$) in the quantum wire limit, while others remain optically active. In both cases,

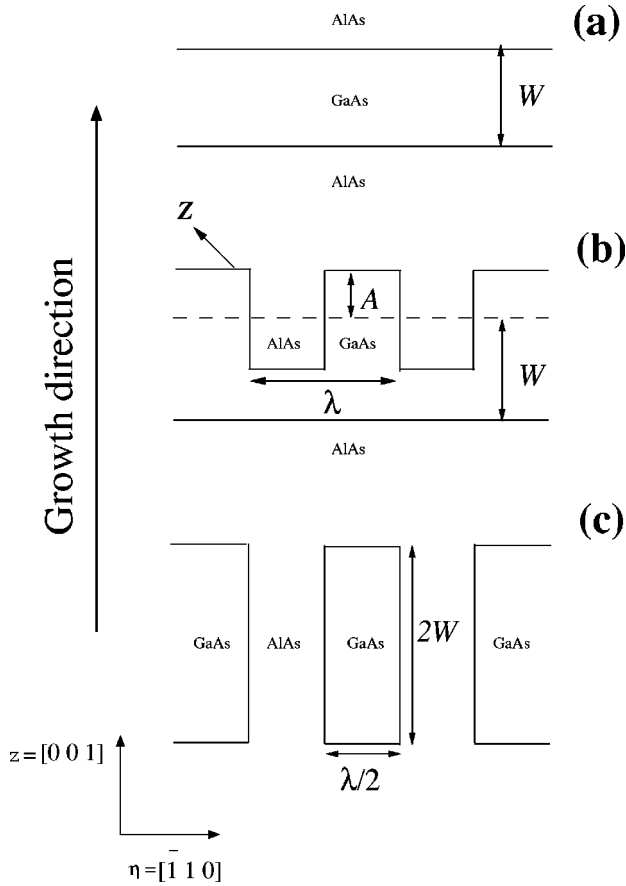


FIG. 1. Schematic illustration of three interface configurations of a AlAs/GaAs/AlAs (001) heterostructure of average width W : (a) QW of width W with completely flat interfaces; (b) QW of average width W (dashed line) with one flat interface and the other given by the step function Z with amplitude A and wavelength λ ; (c) Rectangular quantum wires $2W \times \lambda/2$, corresponding to the limit $A = W$.

clear optical signatures of a quantum well to quantum wire crossover in the electron wave function, induced by interface roughness increase, are identified. The first case is trivial. The crossover is characterized by a direct-to-indirect gap transition. For the last case, we find that the crossover may be identified by a minimum in $f(A)$, the oscillator strength dependence on A .

II. MODEL CALCULATION AND METHOD

We consider GaAs QW's of average width W between wide AlAs barriers, as illustrated in Fig. 1. Figure 1(a) shows the QW structure with planar interfaces, while Fig. 1(b) refers to the steplike QW configuration in which one of the interfaces is planar and the other is defined by a periodic step function Z with amplitude A and wavelength λ . Increasing A one eventually reaches the quantum wire limiting case, $A = W$, depicted in Fig. 1(c). From these configurations we see that increasing A changes the heterostructure geometry progressively from a QW with flat interfaces ($A = 0$) to a rectangular quantum wire ($A = W$) of basal area $2W \times \lambda/2$.

Calculations are performed within a real-space supercell

formalism, with periodic boundary conditions.¹⁶ The supercells geometry is chosen to describe the configurations in Fig. 1, with $W = 16$ ML (monolayers; 1 ML = $a/2$, where a is the conventional cubic cell parameter). By adopting orthorhombic supercells of dimensions N_η , N_ξ , and N_z ($\xi = [1 \ 1 \ 0]$) we model the interface shape with steps along the η direction according to

$$Z(\eta, \xi) = \begin{cases} A & \text{for } kN_\eta < \eta < \left(k + \frac{1}{2}\right)N_\eta \\ -A & \text{for } \left(k - \frac{1}{2}\right)N_\eta < \eta < kN_\eta, \end{cases} \quad (2)$$

where k is an integer, A is the amplitude, and $N_\eta = \lambda$ defines the wavelength of interface oscillations. For this shape function, Eq. (1) gives $\rho = A$. In Sec. III, we use A instead of ρ to quantify the interface deviations from planar geometry. One should notice that the amplitude can only vary within a set of discrete values (multiples of 1 ML) between 0 and $W = 16$ ML.

In AlAs/GaAs heterostructures, Ga or Al atoms occupy one of the two interpenetrating *fcc* sublattices of the zincblende structure, and As atoms occupy the other. Because GaAs and AlAs present negligible lattice mismatch, we assume that, for every configuration, all atoms remain “frozen” at their ideal equilibrium zincblende positions. The electronic states are treated within an approach based on empirical TB theory. We use the first-nearest-neighbor model proposed by Vogl *et al.*,¹⁷ which adopts an sp^3s^* basis set, with the zero energy level corresponding to the Γ state at the top of the valence band of AlAs. For GaAs, we take a positive band offset correction of 0.47 eV.¹⁸ Recent studies¹⁹ have demonstrated that this is a reliable parametrization for the QW's properties investigated here.²⁰ The corresponding spin-independent TB Hamiltonian is

$$H = \sum_{\vec{R}, \alpha} \epsilon_{\vec{R}, \alpha} c_{\vec{R}, \alpha}^\dagger c_{\vec{R}, \alpha} + \sum_{\vec{R}, \alpha, \vec{R}', \alpha'} t_{\vec{R}, \alpha, \vec{R}', \alpha'} c_{\vec{R}, \alpha}^\dagger c_{\vec{R}', \alpha'}, \quad (3)$$

where $c_{\vec{R}, \alpha}^\dagger$, $c_{\vec{R}, \alpha}$ are electron creation and annihilation operators, with $\alpha = s, p_x, p_y, p_z, s^*$ representing the atomiclike basis functions, $\epsilon_{\vec{R}, \alpha}$ the on-site energies, and $t_{\vec{R}, \alpha, \vec{R}', \alpha'}$ the hopping parameters between the indicated orbitals at lattice nearest-neighbor sites \vec{R} and \vec{R}' . The TB eigenfunctions

$$\psi_{TB} = \sum_{i, \alpha} C_{i, \alpha} |\vec{R}_i, \alpha\rangle \quad (4)$$

are characterized by the expansion coefficients $C_{i, \alpha}$. The supercell sizes are defined according to the system geometry with N_z large enough to guarantee convergence of our results to the infinite-width barriers situation. The largest cells involve $N_z = 100$ ML, $N_\xi = 14\sqrt{2}$ ML, and $N_\eta = 28\sqrt{2}$ ML, leading to cells with 78 400 atoms. Since we are interested in electronic properties that involve only the first electron state ($|e_1\rangle$) and the first hole state ($|h_1\rangle$) in the well, H in Eq. (3) is diagonalized using an efficient computational method²¹ that scales linearly in time with the size of the system.

We consider initially a structure with planar interfaces [see Fig. 1(a)]. For a given supercell size in the z direction, N_z , we increase the GaAs well width from $W=0$ (pure AlAs) to $W=N_z$ (pure GaAs). For intermediate W , the imposed periodic boundary conditions generate a $(\text{GaAs})_W(\text{AlAs})_M$ superlattice, with $M=N_z-W$. Since these configurations are translationally invariant in the two directions perpendicular to z , the superlattice eigenstates may be conveniently labeled (according to their symmetry properties) by a \vec{k} vector in a two-dimensional Brillouin zone of the superlattice.¹⁰ A detailed analysis of the \vec{k} symmetry of the band-edge states in GaAs/AlAs QW's and superlattices within the TB formalism was performed in Ref. 19. Since general types of interface roughness completely break the translational symmetry of the system, it is interesting to investigate whether reciprocal-space assignments for the band-edge states will remain useful in the present context. For random alloys, which is also a system with completely broken translational symmetry, we have previously shown¹¹ that the orbital averaged spectral weight

$$\Omega(\vec{k}) = \sum_{\alpha} |C_{\alpha}(\vec{k})|^2 = \frac{1}{N} \sum_{i,j,\alpha} \exp[i\vec{k} \cdot (\vec{R}_i - \vec{R}_j)] C_{i,\alpha} C_{j,\alpha}^* \quad (5)$$

provides a reliable way to quantify the amount of zincblende \vec{k} -symmetry character in the wave functions. We present in Fig. 2(a) the calculated spectral weight at the Γ point for the band-edge states $|e_1\rangle$ and $|h_1\rangle$. Calculations were performed for $N_{\xi}=N_{\eta}=8\sqrt{2}$ ML and three values of N_z : 50, 80, and 100 ML. Note that the conduction-band-edge state has zero spectral weight at Γ for $W=0$, consistent with the AlAs band structure where the conduction-band minimum is at X , so $|e_1\rangle$ has no Γ component. This behavior is maintained while $W < 10$ ML. For the AlAs valence-band-edge state, the full spectral weight is at Γ [i.e., $\Omega_{h_1}(\Gamma)=1$ for $W=0$], again consistent with the AlAs band structure. Calculated values of $\Omega(\Gamma)$, for both states $|e_1\rangle$ and $|h_1\rangle$, and for all other QW widths W , decrease with increasing supercell dimension N_z . Of course this is not an unphysical result: It reflects the increase in the number of k -space sampled points as the supercell size increases for a system where the zincblende \vec{k} vector is not a good “quantum number.”

In Fig. 2(b) we present, for the same supercell configurations, the calculated oscillator strength of the transition between $|e_1\rangle$ and $|h_1\rangle$,

$$f = \frac{2}{m} \frac{|\langle e_1 | \vec{p} | h_1 \rangle|^2}{\Delta E}, \quad (6)$$

where m is the free electron mass, $\langle e_1 | \vec{p} | h_1 \rangle$ the momentum matrix element between states $|e_1\rangle$ and $|h_1\rangle$, and $\Delta E = E(e_1) - E(h_1)$ is their energy difference, which also gives the well's energy gap. The momentum matrix element is calculated through the TB expression²²

$$\langle e_1 | \vec{p} | h_1 \rangle = \frac{im}{\hbar} \sum_{i,j,\alpha,\beta} C_{i,\alpha}^e C_{j,\beta}^h H_{i\alpha,j\beta} \vec{d}_{i,j}, \quad (7)$$

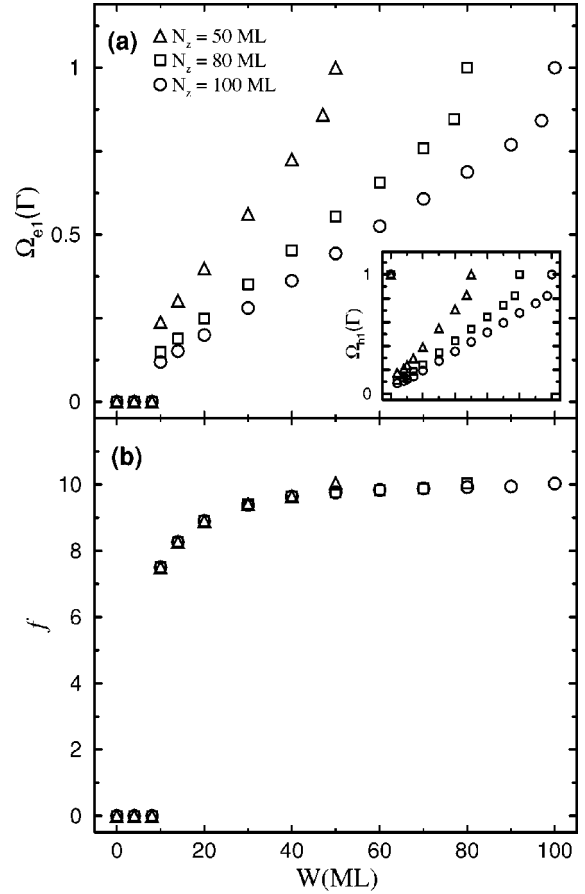


FIG. 2. (a) Spectral weight at the zincblende Γ point calculated with different values of the supercell dimension N_z . Data points correspond to the band-edge states, $|e_1\rangle$ and $|h_1\rangle$ (latter given at the inset), for a $(\text{GaAs})_W(\text{AlAs})_{N_z-W}$ superlattice, as a function of the GaAs width W . (b) Oscillator strength f for the same superlattices.

where $C_{i,\alpha}^e$, $C_{j,\beta}^h$ are the expansion coefficients for $|e_1\rangle$ and $|h_1\rangle$ and $H_{i\alpha,j\beta}$ is the Hamiltonian matrix element relative to basis orbitals $|\vec{R}_i,\alpha\rangle$, $|\vec{R}_j,\beta\rangle$, and $\vec{d}_{i,j} = \vec{R}_j - \vec{R}_i$. As expected from the results in (a), f vanishes in the indirect-gap regime $W < 10$. Also, f depends only on the QW geometry, not on N_z . This is a crucial feature for QW studies since, for each particular interface geometry, N_z is taken to be large enough to guarantee convergence of the results to the infinite-width barriers situation.²³ According to this criterion, the oscillator strength, as well as the transition energy ΔE or the momentum matrix element, are reliable quantities while the spectral decomposition of the band-edge states will not provide further insight into the problem. In what follows we characterize the optical properties of the QW's by the oscillator strength of the main gap transition.

III. RESULTS FOR THE OPTICAL PROPERTIES

Results for QW's with flat interfaces in Fig. 2 show that narrow wells display indirect-gap behavior (dipole-forbidden transitions, $f=0$) and a sharp transition into direct gap (dipole-allowed transitions, $f \neq 0$) occurs for $W=10$ ML. Therefore, for the value of W considered here (16 ML) and in

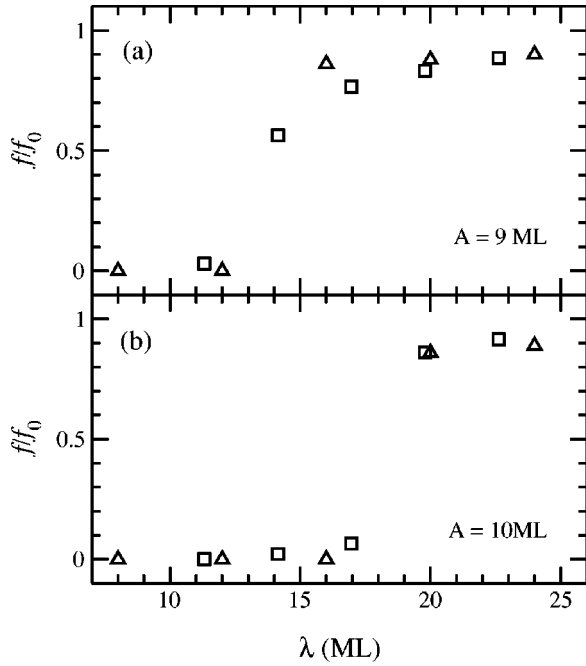


FIG. 3. Calculated variation of the oscillator strength of QW's illustrated in Fig. 1 as a function of the interface modulation wavelength λ . The results correspond to average width $W = 16$ ML and the indicated values of interface modulation amplitude A , and are normalized with respect to the flat interface value. Triangles (squares) represent step formation in the $x = [100]$ ($\eta = [\bar{1}10]$) direction.

the absence of interfaces roughness, the first optical transition in the well is dipole allowed.

Figure 3 gives the oscillator strength f normalized to the flat interface value f_0 as a function of the interface wavelength λ for fixed values of the amplitude, (a) $A = 9$ ML and (b) $A = 10$ ML. Triangles and squares, which are essentially superimposed, correspond to steps formation along the x and η directions, respectively. The calculated optical behavior is, therefore, independent of the direction of the steps: This provides additional confirmation for the main conclusion in Ref. 15, namely, that the only relevant parameter is the interface roughness, which is of course isotropic for steps formed along any crystalline direction. It is also clear that, for these amplitudes, decreasing λ leads to a transition from direct-to-indirect gap behavior at a value of λ that depends on the amplitude A : It occurs at $\lambda \sim 15$ ML for $A = 9$ ML and $\lambda \sim 20$ ML for $A = 10$ ML. This transition is indicated by the solid line in Fig. 4, where a phase diagram for the overall optical behavior of the $W = 16$ ML system is presented.

Figure 5 further explores the combined effects of interface modulations amplitude and wavelength. It presents results for the oscillator strength as a function of A , $f(A)$, for different values of λ . For $\lambda = 8\sqrt{2}$ ML (diamonds) and $12\sqrt{2}$ ML (squares), the oscillator strength decreases with increasing A , and eventually undergoes a transition to zero. This qualitative behavior is exactly the same obtained for $\lambda = 8$ ML in Ref. 15. As noted above (Fig. 3), increasing λ increases the amplitude at which the direct-to-indirect transition occurs. However, a new situation is encountered when

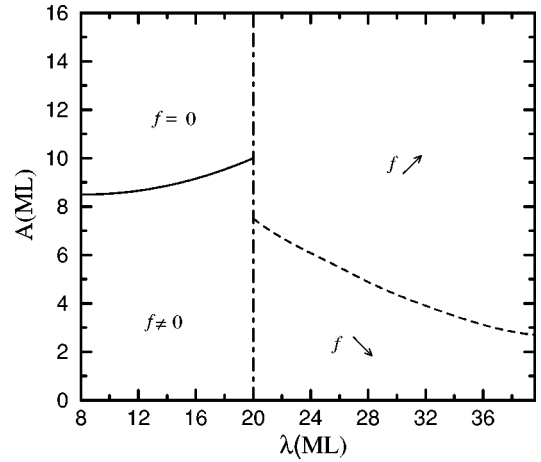


FIG. 4. Phase diagram illustrating the optical behavior of AlAs/GaAs/AlAs heterostructures as a function of the interface modulation geometric parameters for $W = 16$ ML. The dash-dot line separates *short* (left) from *long* (right) periodicity, the solid line indicates direct ($f \neq 0$) -to-indirect ($f = 0$) gap transitions while the dashed line separates QW-like ($f \searrow$) from quantum-wire-like ($f \nearrow$) optical behavior. Due to the discrete nature of the parameters A and λ , the lines in this diagram indicate average values where the cross-overs between different behaviors take place.

λ is sufficiently large, e.g., $\lambda = 14\sqrt{2}$ ML (circles in Fig. 5): No transition to $f = 0$ occurs, and a peculiar optical behavior is found. As A increases from 0, the calculated oscillator strength decreases as described above, attaining a sharp minimum at $A \approx 8$ ML, above which f increases with A up to $A = W$. For $\lambda = 28\sqrt{2}$ ML (triangles), the minimum in $f(A)$ occurs at $A \approx 3$ ML. Thus, when A increases from 0 to W , the system may display two different optical behaviors depending on λ . We may refer to the modulation periodicity as *short* or *long* according to these behaviors: (i) for *short* periodicity the system is optically active in the quantum well regime and becomes inactive in the quantum wire limit; (ii) for *long* periodicity, both regimes are optically active and $f(A)$ has well defined minimum. In Fig. 4, *short* (*long*) periodicity behavior is found to the left (right) of the vertical dash-dot line. In the *long* periodicity region, the minimum in $f(A)$ is indicated by the dashed line, which separates the decreasing ($f \searrow$) and increasing ($f \nearrow$) ranges of $f(A)$.

Of course the values of λ defining *short* or *long* periodicity behavior depend on the width W . The minimum basal area leading to optically active quantum wires, from our results in Fig. 5, is $W \times \lambda \approx 2.48 \times 10^3 \text{ \AA}^2$. It is interesting to note that this estimate is in good agreement with the theoretical result of Franceschetti and Zunger²⁴ based on an empirical pseudopotential approach. They found that the critical diameter for the direct-to-indirect band-gap transition is 56 \AA in a GaAs cylindrical quantum wire embedded in AlAs, which corresponds to critical basal area of $2.46 \times 10^3 \text{ \AA}^2$.²⁵

In order to investigate qualitatively the peculiar optical behavior obtained in the *long* periodicity regime, we explore the electronic TB wave function. The overall probability den-

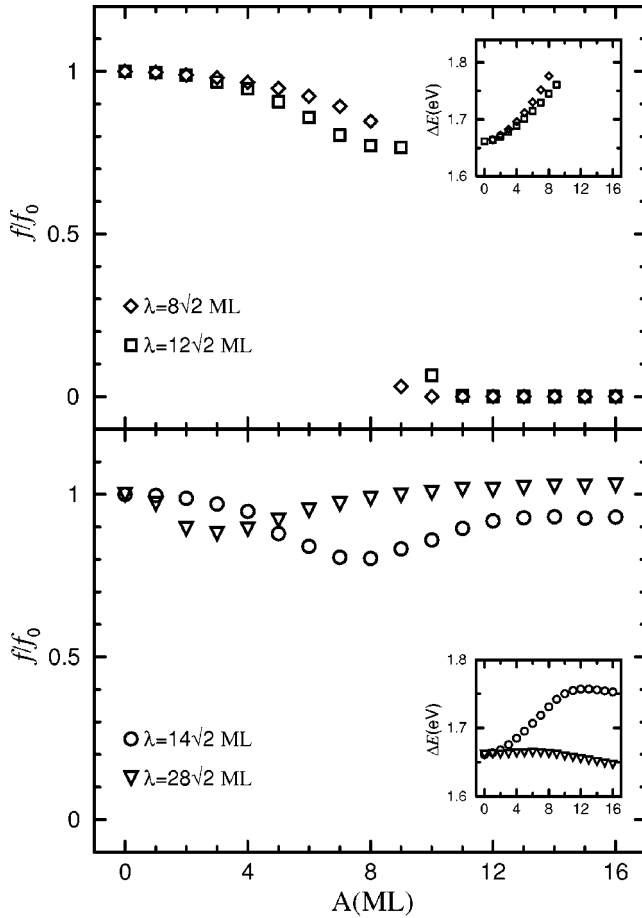


FIG. 5. Calculated variation of the oscillator strength of QW's of average width $W=16$ ML, illustrated in Fig. 1, as a function of the interface amplitude A . The oscillator strength is normalized to the flat interface values. Different symbols correspond to the indicated modulation wavelengths. The insets give the corresponding energy gaps ΔE in the direct-gap range.

sity distribution across the well may be described through the envelope function¹¹ $|\psi_{EF}(\eta, z)|^2$, which corresponds to the projected squared TB coefficients (summed over orbitals, sublattices and coordinate ξ) in the η, z plane. Figure 6 illustrates the electronic density distribution corresponding to the state $|e_1\rangle$ for a QW of average width $W=16$ ML, for interface modulation periodicity $\lambda=14\sqrt{2}$ ML, and for different values of the amplitude. The amplitudes $A=0$ and 4 ML correspond to the $f \searrow$ regime, while $A=8, 12$, and 16 ML to the $f \nearrow$ regime. These particular amplitudes are represented by the filled circles in Fig. 6(a). In Figs. 6(b)–6(f) we present $|\psi_{EF}(\eta, z)|^2$ by the gray-scale plots, where darker regions correspond to higher charge densities.

For the QW with $A=0$, $|\psi_{EF}(\eta, z)|^2$ is homogeneously distributed along η in the GaAs region. For $A=4$ ML, we note a displacement of the electronic density away from the rough interface, with an overall behavior similar to the flat interface distribution, but in a narrower QW.¹⁵ We obtain a qualitatively different behavior for $A=8$ ML: The charge distribution becomes highly inhomogeneous along η , with appreciable migration of the electronic density to the wider GaAs valleys, and away from the AlAs constrictions into the

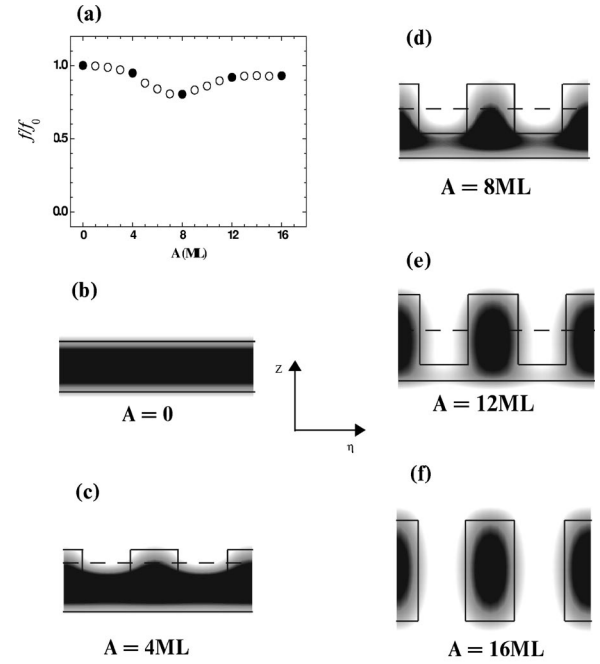


FIG. 6. (a) Same as Fig. 5 for $\lambda=14\sqrt{2}$ ML. (b)–(f) Envelope wave function squared, projected in the ηz plane, for the first electron state in the QW's. The considered interface modulation amplitudes are indicated in (a) by the filled circles: (b) $A=0$; (c) $A=4$ ML; (d) $A=8$ ML; (e) $A=12$ ML; (f) $A=16$ ML. The gray scale indicates higher densities by darker regions. Solid and dashed lines represent the interfaces geometry, as in Fig. 1.

QW. Further increasing the amplitude causes the electron state $|e_1\rangle$ to remain predominantly localized in the wider GaAs valleys, with negligible density around the AlAs steps. This reveals an electronic distribution approaching the quantum wire limit, $A=W=16$ ML. Therefore, it is plausible to identify the two regimes in the calculated f with a predominantly quantum well ($f \searrow$) or quantum wire ($f \nearrow$) character of the electronic charge distribution in the GaAs region. In this context, the amplitude corresponding to the oscillator strength minimum is identified with a characteristic amplitude above which the system crosses over to the quantum wire regime. For *long* λ , the calculated oscillator strength minimum provides an optical signature for the crossover from two-dimensional to one-dimensional electronic distribution with increasing A .

It is simple to understand, in general terms, the origin of the $f \searrow$ and $f \nearrow$ regimes of $f(A)$. Starting from the perfect QW limit $A=0$, it is known that increasing the interface roughness is equivalent to narrowing the well,¹⁵ so $f(A)$ is a decreasing function of A for $A \sim 0$. In the quantum wire limit, $A=W$, the oscillator strength is enhanced by confinement, which increases the real-space overlap of the electron and hole states, leading to larger optical matrix elements. Note in Fig. 5 that for $\lambda=28\sqrt{2}$ ML (triangles), $f(W)$ is even larger than $f(0)$. In the quantum wire limit, decreasing A from W reduces the confinement, thus reducing f . This justifies associating the $f \searrow$ and $f \nearrow$ regimes respectively to QW-like and quantum-wire-like optical behavior of the system, with the crossover identified by the minimum in $f(A)$.

The behavior of the energy gap versus A , presented in the insets in Fig. 5, shows that in the QW regime the energy increases monotonically with A , while in the quantum wire regime it saturates. Thus the crossover might also be inferred from the behavior of ΔE vs A . However, for large enough λ , e.g., $\lambda = 28\sqrt{2}$ ML in Fig. 5, ΔE is not a very sensitive function of A , while a minimum in f vs A may still be clearly identified.

IV. SUMMARY AND DISCUSSIONS

By employing a real-space supercell formalism we have investigated interface modulation effects on the optical properties of AlAs/GaAs/AlAs QW's. Interface modulations are modeled, in only one of the interfaces, by periodic steps of amplitude A and wavelength λ . For a given λ , increasing A from 0 to the well width means changing the geometry from a QW with flat interfaces into a quantum wire of rectangular basis. The optical nature of the heterostructures is studied by calculating the oscillator strength of the fundamental transition in the QW's. We found characteristic behaviors for the oscillator strength with increasing A . For *short* λ a direct-to-indirect band-gap transition takes place while, for sufficiently *long* λ , this transition does not occur. In this last case, the gap remains direct at all amplitudes, with the oscillator

strength presenting a minimum value at an intermediate amplitude. For *long* λ , we associate the oscillator strength minimum with the optical signature of the crossover from two-dimensional to one-dimensional optical behavior.

Of course the shape of the interface modulations adopted here is important in defining the lower-dimension geometry in the limit when the modulation amplitude approaches the QW width. Steps or other oscillations restricted to one particular direction perpendicular to z lead to quantum-wire-like geometries in this limit. However, for more general types of oscillations in the x - y plane, amplitude modulations increase may lead to quantum dots formation. The behavior obtained here is also expected to occur in the islands formation processes, where quantum confinement effects are known to enhance the optical efficiency of the system.

ACKNOWLEDGMENTS

The authors would like to thank H. Chacham, L.A. Cury, and F.J. Ribeiro for helpful discussions and suggestions. This work was partially supported by the Brazilian agencies Fundação de Amparo à Pesquisa do Rio de Janeiro (FAPERJ), Conselho Nacional de Desenvolvimento Científico e Tecnológico (CNPq), MCT-PRONEX, and Fundação Universitária José Bonifácio (FUJB).

-
- ¹W. Braun and K.H. Ploog, J. Appl. Phys. **75**, 1993 (1994).
²W. Braun, A. Trampert, L. Daweritz, and K.H. Ploog, Phys. Rev. B **55**, 1689 (1997); K.H. Ploog, J. Cryst. Growth **174**, 522 (1997).
³M. Kozhevnikov, E. Cohen, and A. Ron, Phys. Rev. B **60**, 16 885 (1999).
⁴C-Y Mou and T-M Hong, Phys. Rev. B **61**, 12 612 (2000).
⁵A. Zrenner, L.V. Butov, M. Hagn, G. Abstreiter, G. Bohm, and G. Weimann, Phys. Rev. Lett. **72**, 3382 (1994).
⁶D. Gammon, E.S. Snow, B.V. Shanabrook, D.S. Katzer, and D. Park, Science **273**, 87 (1996).
⁷K. Leosson, J.R. Jensen, W. Langbein, and J.M. Hvan, Phys. Rev. B **61**, 10 322 (2000).
⁸M. Yoshita, N. Kondo, H. Sakaki, M. Baba, and H. Akiyama, Phys. Rev. B **63**, 075305 (2001).
⁹F. Capasso *Physics of Quantum Electron Devices* (Springer, Berlin, 1990).
¹⁰G. Bastard *Wave Mechanics Applied to Semiconductor Heterostructures* (Les Éditions de Physique, Paris, 1988).
¹¹T.G. Dargam, R.B. Capaz, and B. Koiller, Phys. Rev. B **56**, 9625 (1997).
¹²B. Koiller, R.B. Capaz, and H. Chacham, Phys. Rev. B **60**, 1787 (1999).
¹³B. Koiller, A.S. Martins, and H. Chacham, Appl. Phys. Lett. **69**, 2423 (1996).
¹⁴R.B. Capaz, T.G. Dargam, A.S. Martins, H. Chacham, and B. Koiller, Phys. Status Solidi A **173**, 235 (1999).
¹⁵T.G. Dargam and B. Koiller, Solid State Commun. **105**, 211 (1998).
¹⁶B. Koiller and R.B. Capaz, Phys. Rev. Lett. **74**, 769 (1995).
¹⁷P. Vogl, H.P. Hjalmarson, and J.D. Dow, J. Phys. Chem. Solids **44**, 363 (1983).
¹⁸A.D. Katnani and R.S. Bauer, Phys. Rev. B **33**, 1106 (1986); C.G. Van de Walle and R.M. Martin, J. Vac. Sci. Technol. B **4**, 1055 (1986); S. Massida, B.I. Min, and A.J. Freeman, Phys. Rev. B **35**, 9871 (1987).
¹⁹J.G. Menchero, T.G. Dargam, and B. Koiller, Phys. Rev. B **61**, 13 021 (2000).
²⁰D.J. Chadi and M.L. Cohen, Phys. Status Solidi B **68**, 405 (1975). As discussed there, sp^3 nearest-neighbor models are not appropriate for studying the X state because they give a dispersionless band structure between the X and W points. This limitation also applies to sp^3s^* nearest-neighbors models. In Ref. 19 it is shown that Vogl's sp^3s^* parametrization Ref. 17 is reliable to describe the whole direct-gap regime of GaAs/AlAs QW's, and to determine the critical width at which a direct-to-indirect gap transition occurs.
²¹R.B. Capaz, G.C. de Araujo, B. Koiller, and J.P. von der Weid, J. Appl. Phys. **74**, 5531 (1993).
²²B. Koiller, R. Osório, and L.M. Falicov, Phys. Rev. B **43**, 4170 (1991).
²³L.C. Lew Yan Voon and L.R. Ram-Mohan, Phys. Rev. B **47**, 15 500 (1993).
²⁴A. Franceschetti and A. Zunger, Phys. Rev. B **52**, 14 664 (1995).
²⁵This agreement confirms the reliability of Vogl's parametrization for the present study.